Materials Today: Proceedings xxx (xxxx) xxx

Contents lists available at ScienceDirect

Materials Today: Proceedings

journal homepage: www.elsevier.com/locate/matpr

Aerosol Jet® printing 3D capabilities for metal and polymeric inks

Miriam Seiti, Olivier Degryse, Eleonora Ferraris *

Manufacturing Processes and Systems (MaPS), Mechanical Engineering, KU Leuven, Sint Katelijne Waver 2860, Belgium

ARTICLE INFO

Article history:
Available online xxxx

Keywords:
Aerosol Jet® Printing
3D microstructures
Micropillars
Microlattices

ABSTRACT

Aerosol Jet® printing (AJ®P) is a direct writing printing technology which deposits functional aerosolized solutions on free-form substrates. Its potential has been widely adopted for two-dimensional (2D) micro-scale constructs in printed electronics (PE), and it is rapidly growing toward surface structuring and biological interfaces. However, limited research has been devoted to its exploitation as a three-dimensional (3D) printing technique. This paper investigates 3D AJ®P capabilities of three inks along with a comparison of their abilities and limitations by employing three AJ®P 3D strategies (continuous jet deposition, layer-by-layer, point-wise). In particular, 3D microstructures of increasing complexity based on a silver nanoparticle (AgNPs)-, a poly(3,4-ethylenedioxythiophene)polystyrene sulfonate (PEDOT:PSS)-, and a collagen-based ink are here investigated at various aspect ratios and resolutions. Results show the possibility to print not only arrays of micro-pillars of different aspect ratios (AgNPs-ARs $\sim$ 20, PEDOT:PSS-ARs $\sim$ 7, collagen-ARs $\sim$ 3), but also dense and complex (but low reproducible) leaf- or flake-like structures (especially in AgNPs), and lattice units (collagen). This study demonstrates that the fabrication of 3D AJ® printed microstructures firmly depend on the printing parameters and the ink (co–)solvents fast-drying phenomena during printing. Moreover, it provides guidelines about ink development and print strategies for 3D AJ®P micro-structuring, opening its adoption in a vast range of applications in life science (tissue engineering, bioelectronic interfaces), electronics, and micromanufacturing.

Selection and peer-review under responsibility of the scientific committee of The International Conference on Additive Manufacturing for a Better World.

1. Introduction

Microfabrication processes for high aspect ratio (AR) three-dimensional (3D) structures have been widely investigated since the beginning of XXI century. In particular, the micro-forming process aims to produce semi-planar or 3D structures from nanometers to sub-millimeters scales.[1] As reported by Vaezy et al. [2], many traditional and state-of-the-art processes are currently accessible from subtractive lithography-based, additive manufacturing (AM)-based, and hybrid-based approaches. The range of applications is in continuous expansion, ranging from electronics and life science to aerospace and automotive. In particular, 3D periodic microstructures, such as arrays of pillars or lattice units, with well-defined geometrical characteristics (aspect ratio (AR), diameter, height, and inter-spacing), have been efficiently used for micro-electromechanical systems (MEMS), energy harvesting 3D micro-batteries, bioinspired architectures, micro-sensors (electrochemical sensing, micro-actuators), micro-optical devices, circuit packaging, etc [3–5]. In life science, 3D periodic microstructures have also been embedded in bacterial sensors, scaffold-based cell culture systems for guiding and cell growth, electrophysiological recording sensors, and microbial electrolytic cell [6–8].

In the case of additive manufacturing, 3D structures are produced by direct printing through a functional (multi)-material deposition process. Among AM techniques, Aerosol Jet® Printing (AJ®P) was introduced in the early 90 s by Optomec© Inc. (USA), mainly for printed electronics (PE) applications on *free-form* (e.g. flat/curved, rigid/flexible) substrates. Being part of the direct writing (DW) category, AJ®P enables the deposition of (multi-) functional materials in the form of an aerosol through a nozzle at a variable stand-off distance, z [1–5] mm, from the substrate. The result is a well-defined printed pattern, with a minimum feature size starting from 15 μm up to few cm in width and 0.1 μm in thickness. Two-dimensional (2D) applications have been extensively reviewed mainly for PE, such as antennas, batteries, smart packaging, and sensors [9]. Despite an increasing interest in

* Corresponding author.
E-mail address: eleonora.ferraris@kuleuven.be (E. Ferraris).

https://doi.org/10.1016/j.matpr.2022.08.488
2214-7853/
Selection and peer-review under responsibility of the scientific committee of The International Conference on Additive Manufacturing for a Better World.

research and several emerging applications in bioelectronics [10], surface structuring, and biological interfaces [11], the exploitation of this technology as a 3D printing technique is still very limited, and only a couple of examples have reported in the literature.

Saleh et al. was the first to AJ® print silver nanoparticles (AgNPs)-based fully dense truss elements, like lattices and micropillars arrays at high ARs ~ 20 [12]. Zips et al. also AJ® printed a composite of poly(3,4-ethylenedioxythiophene) polystyrene sulfonate (PEDOT:PSS) and multiwalled carbon nanotube ink with an AR ~ 3.3 [13]. Finally, Hohnholz et al. and Di Novo et al. explored the use of photo-reactive polymers, such as Polydimethylsiloxane (PDMS) and ultra-violet (UV)-curable adhesives to reach 3D printed structure with AJP [14,15]. In each case, the ink formulation and print parameters were controlled and adapted for the specific application. However, these works are dictated by trial-and-error explorations and they lack a thorough investigation on 3D AJ®P capabilities and limitations, associated to different inks formulations.

This paper aims at fulfilling this research gap with the purpose to identifying preliminary guidelines for AJ®P of 3D microstructures of increasing complexity, with respect to materials and print strategies. Three inks, among which Newtonian and non-Newtonian fluids, that drastically differentiate in ink composition and application functionality (electronics, bioelectronics and biological interfaces) and three print strategies are here selected and combined to realise 3D printed structures of different complexity and aspect ratios.

This work is the first to provide a systematic discussion on 3D AJ®P capabilities for different ink compositions and print strategies, and it highlights the ability of AJ®P as a 3D microfabrication technology, emphasizing its future use for 3D micromanufacturing, electronics, and life science.

2. Material and methods

2.1. Fundamentals of AJ®P and ink formulation

AJ®P is a direct writing, nozzle-based technique which allows the atomization and deposition of a (multi)-functional ink on a *free-form* substrate, at high micro-scale resolutions and accuracy. In an ultrasonic configuration (U-AJ®P), a functional ink is atomized into a mist, which is then accelerated through a carrier gas flow (*CGF*, [0–50] sccm) (generally an inert gas, such as N_2) into a transport tube till the deposition head. Here, the aerosol beam is collimated and aerodynamically focused in the nozzle by an annular gas flow, known as sheath gas flow (*SGF*, [0–200] sccm), typically N_2. Afterwards, the jet exits from the nozzle (i.e. in-flight jet) and then impacts on the desired substrate. Eventually, a post-process step is applied to cure or crosslink the printed structure. Fig. 1 depicts the *AJ®P* technique, divided into its three physical sub-processes: i) Atomization and Transport, ii) Collimation & In-flight Jet, and iii) Impaction & Impingement [16], according to a selected print strategy: continuous jet deposition, layer-by-layer, and point-wise, as explained in *Section 2.3*.

Typical AJ®P functional inks are defined as stable solutions or nano-dispersions (colloids) with a viscosity, η, in the range of [1–1000] mPas (10–20 mPas for U-AJ®P) and surface tension, σ, around [20–75] mN/m. Three elements are typically distinguished: i) a loading content; ii) a (co–)solvent systems, and iii) additives. Standard loading contents are conductive metal (Ag, Cu, Au, Pt) nanoparticles (NPs), with a maximum loading content of 40–60 wt% and an average particle size of 50 nm (U-AJ®P) [17]. Polymeric particles (e.g. PEDOT:PSS) at variable concentration and size are also widely used. Novel inks currently under research can include ceramics, such as hydroxyapatite (HAp), or biomolecules. The ink co-solvent system comprises a main solvent and co-solvents. The former is a liquid medium (usually water at 20–60 v/v% for U-AJ®P), which suspends the particle loading and evaporates during the in-flight jet, impaction, and (thermal) post-process. The latter is instead a combination of co-solvents chosen to control ink atomisation, wetting, evaporation rate during printing, and/or to target specific needs. Their concentrations (usually 5–20 v/v%) mostly depend on volatility (boiling point and vapor pressure), and viscosity. Particularly, highly volatile co-solvents (e.g. alcohols) support the mist transport by the CGF from the vial to the tube [18], while less volatile ones act as humectants during the transport, in-flight and impaction, to avoid fast drying of the printed ink, which typically results in impaired print-quality[16]. Eventually, additives (e.g. surfactants, stabilizers, binders, crosslinkers, initiators and/or functional compounds) can be incorporated based on the target application.

2.2. Inks and substrates preparation

Three aqueous inks were selected as U-AJ®P materials, among which a non-Newtonian commercial AgNPs-based ink (Novacentrix, USA), an own-formulated PEDOT:PSS-based pseudo-elastic dispersion (Sigma Aldrich, Belgium), and a Newtonian own-developed collagen-based solution. Table 1 reports the main features for each of the fluid. The AgNPs-based ink was investigated in its standard formulation and in a diluted form with distilled (DI) water, in a ratio of 1:4. The PEDOT:PSS-based ink was analyzed in its standard commercial solution and as an own-formulated composition. In addition, a collagen and collagen composite ink were formulated by dissolving freeze-dried collagen type I in 0.01 M Hydrochloric acid (HCl) at a concentration of 3 mg mL^{-1}. The collagen was extracted according to a previously published protocol [19]. The composite ink was prepared for use in bone tissue applications. Hence, HAp was added to the collagen solution as particle loading by adding 6 % v/v of a 10 wt% aqueous HAp suspension (<200 nm; Sigma Aldrich, BE), as this 1:2 collagen to HAp ratio mimics the composition of human bone tissue. Glass slides (Superfrost or Micro cover glasses, VWR, BE) were selected as reference substrate and ultrasonically cleaned at T = 25 °C (EMMI – 20 HC, Emag) for 10 min prior to use, with a mixture of distilled water (DI) and 2-propanol (IPA, Sigma Aldrich, BE). Before printing, the conductive inks were ultrasonically sonicated for 10 min at 25 °C. On the other hand, for the collagen inks, glass cover slips (Ø12 mm, VWR, Belgium) were used as the reference substrate, and were cleaned in an ultrasonic bath using MilliQ water and ethanol, before being stored in a 1X phosphate buffered saline (PBS; Lonza, BE) in order to remove any surface charges. The collagen inks could not be ultrasonically homogenized as this would result in degradation of the collagen molecule, as shown by Gibney et al. [19].

2.3. AJ®P tools and experimental methodology

An Optomec AJ®P 300 s system equipped with an ultrasonic atomizer (U-AJ®P) was used to print samples. Three 3D AJ®P printing strategies, i) a continuous jet deposition (CJD), ii) a traditional layer-by-layer (LBL), and iii) a point-wise (PW) approach, were exploited. CJD is a continuous deposition of the aerosol jet on a given spot, while LBL is the traditional layer-by-layer printing in a pattern. Finally, PW is a spot-by-spot of the aerosol jet in a pattern. Unlikely, LBL and PW, CJD does not require the use of a shutter and a print speed, s [mm/*sec*]. For each strategy, the nozzle was settled at a stand-off distance, z [mm], of 3 mm. For CJD, a continuous deposition of aerosolized material on a single spot was performed with the aim to realize 3D high ARs pillars. In the LBL approach, the targeted samples were arrays of 6x4 pillars, each

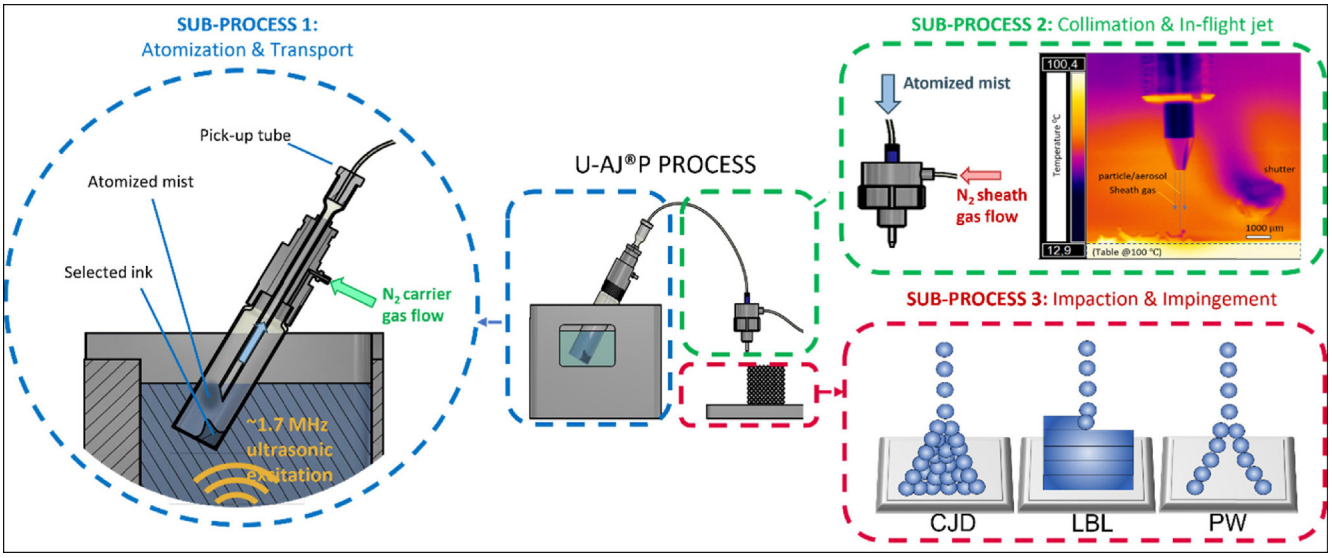

Fig. 1. The AJ®P process in ultrasonic configuration (U-AJ®P), divided into the three physical sub-processes: i) Atomization and Transport, ii) Collimation & In-flight Jet, and iii) Impaction & Impingement according to a specific printing strategy among i) continuous jet deposition (CJD), ii) layer-by-layer (LBL), and iii) point-wise (PW) approach.

Table 1
AJ®P inks selected for the print investigation of 3D microstructures, and related features: i) an AgNPs-based ink for electronics, ii) a PEDOT:PSS-based ink for bioelectronics, iii) and a collagen-based ink for biological interfaces.

AJ®P Inks and Features			
Ink	Metal-based	Polymer-based (synthetic)	Polymer-based (natural)
Supplier	Novacentrix Metalon® JS-A221AE (USA)	Sigma Aldrich (BE) and own-developed formulation	Enzyme extracted Bovine Collagen Type I [3 mg mL^{-1}] supplemented with hydroxyapatite nano-particles
Abbreviation	AgNP-based ink	PEDOT:PSS-based ink	Collagen-based ink
Type	Nano-dispersion		Solution
Density, ρ [g/cm^3]	–	~ 1	~ 1
Viscosity, η [mPas]	5.9	≤ 10	100–150
Surface tension, σ [mN/m]	35.2	75	76
Main Solvent	DI water	DI water	0.01 M HCl
Co-solvents	Diethylene glycol (≥3 - ≤ 10 v/v%) Isopropyl alcohol (≥2 - ≤ 10 v/v%)	Own-formulation: Polyethylene glycol and Ethylene glycol	Glycerol (1 M)
Loading particle	35 nm $Ø_{avg}$ (50 wt%)	PEDOT:PSS, (1.3 wt%)	200 nm $Ø_{avg}$ Hap (3–6 mg/mL)
Additives	–	Carboxymethyl cellulose	1 M glycerol
Notes (Sheet resistance, Rs [Ω/sq])	Conductivity Rs = 50–100 mΩ/ sq	Conductive, Rs = 19–24 Ω/sq	Bioactive and osteoconductive ink

one detected as a circle of 50 µm in diameter. The geometry was designed using AutoCAD software (Autodesk, USA) and then converted in a.prg toolpath code compatible with the printer using VM Tools (VMware, USA). The PW approach was instead used to realize lattice units of pyramidic shape. A MatLab script was created which controlled the shutter opening time (in milliseconds, ms) as well as the position of the print table. Accordingly, the print head moves in a square-shaped sequence and stops at the corners where the shutter opens for a short period (50 to 100 ms), before moving to the next point. By decreasing the square dimensions by each layer, the corner-points ultimately coincide in the center, generating a pyramid. By using a slow printing speed (s = 0.01 mm/s), the deposited material is allowed to dry, providing a supporting surface for the consecutive printed layer.

Table 2 discloses the print parameters and print strategy used for each ink (ambient conditions 22 °C, 55 %rh). Every parameter was selected after a trial-and-error screening for 3D printing, with as output of interest: i) the plate temperature, T [°C], which facilitates drying out and pre-sintering, and ii) the focusing ratio, R_f [#], that is the ratio between SGF and CGF, which regulates the jet focusing during in-flight and evaporation rate upon deposition. R_f also avoids a common phenomenon in AJ®P: the overspray (OS), that is undesired material deposited in the form of porous drops or streams along the printed pattern. For each ink, a homogenous aerosol mist was obtained in at least 15 min after starting the U-AJ®P atomization. Afterall, 10 min were exploited to reach the deposition of a stable ink, before starting printing. In case of using a heated platen, the substrates were allowed to reach thermal equilibrium by placing them on the platform for 10 min. After printing, a post-process was executed based on the selected ink. In detail, a thermal sintering (200 °C, 1 h) and a thermal annealing (140 °C, 1 h) process, were respectively pursued on AgNPs- and PEDOT:PSS-based inks (Heraeus, DE) to ensure full evaporation of the co-solvents and particle aggregation. The collagen samples normally also undergo crosslinking post-printing using a chemical crosslinking approach reported by Gibney et al. [19] However, the crosslinking of collagen was out of the scope of this work.

Each experiment was repeated at least 3 times. Visual inspection and geometrical analyses were performed using an optical microscope (Hirox KH8700) or a scanning electron microscope

Table 2
AJ®P print parameters used for the print investigation for 3D microstructures, divided for ink type.

	Print parameters (23 °C, 50 % rh)			
Printer and Offset, z [mm]	Optomec AJ300s (USA), 3 mm			
Ink	AgNPs-based or water-diluted (1:4) ink, 1 mL		PEDOT:PSS-based (standard and own-formulated) ink, 850 µL	Collagen-based ink
Substrate	VWR Superfrost Glass Slides			VWR Cover Glasses
Printing strategy	CJD	LBL	CJD or LBL	CJD, LBL or PW
Nozzle, Ø [µm]	300	100	150	150
Focusing Ratio, R_f = SGF/CGF	40:10	30:18	35:18	40:19
Platen temperature, T [°C]	40	100	80	37
Printing speed, s [mm/*sec*]	0	0.4	0.4	0 (CJD) 0.4 (LBL) 0.01 (PW)
Printed patterns	CJD-not required / LBL: 6x4 array, Ø = 50 µm			Pillars (Ø = 50 µm) and pyramids
Number of layers, n [#]	1	50	50	50 (LBL)
Post-processing	Thermal sintering (200 °C, 1 h)		Thermal annealing (140 °C, 1 h)	Chemical cross-linking (EDC-NHS)

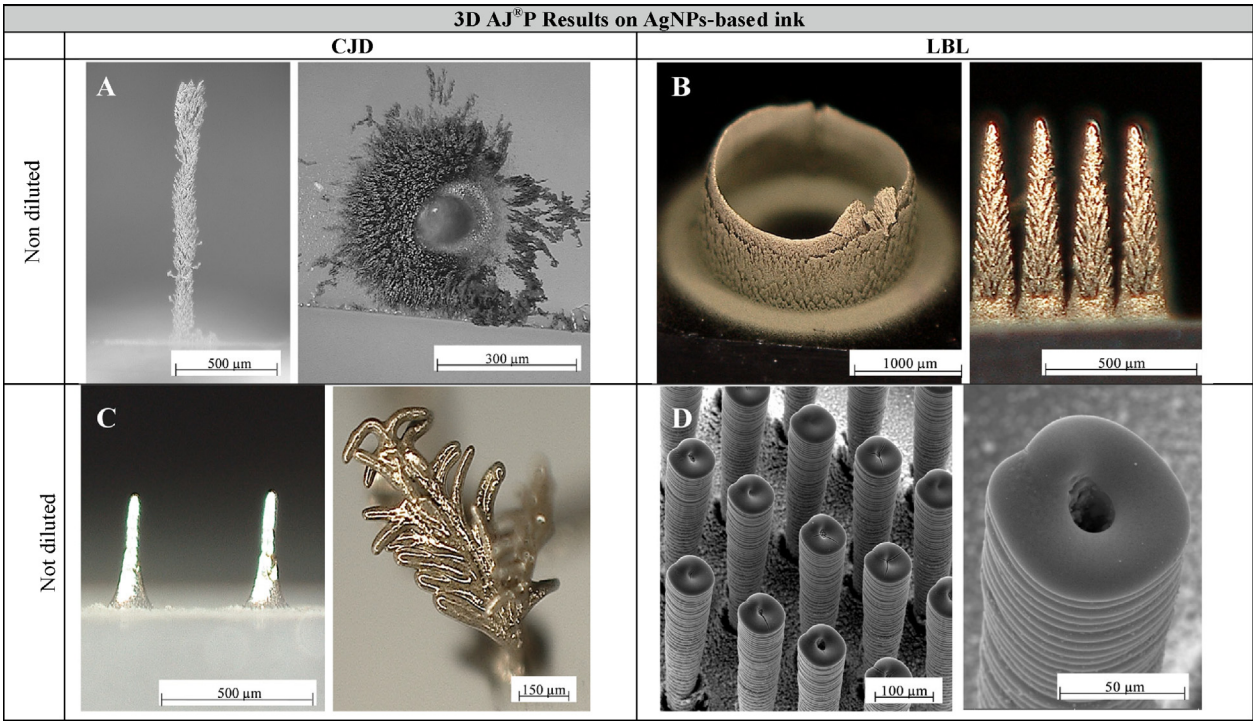

Fig. 2. Results for the 3D AJ®P of microstructures for AgNPs-based ink, along with print strategy and characterization.

(SEM) (Tescan Vega 3, Czech Republic). Particularly, the final shapes were inspected in terms of height, h [µm], width base-tip, w [µm], AR, internal structure (bulk, hollow), process reproducibility (low, medium, high), and printing time, t [secs].

3. Results

3.1. AgNPs-based ink

Fig. 2 illustrates the results of AJ®P AgNPs-based inks. Not diluted and diluted solutions were both investigated for 3D-CJD and 3D-LBL printing of microstructures according to the print parameters of Table 2. It is observed that not diluted AgNPs-based ink generates dendritic-like structures with a rough surface. Instead, the diluted version gives rise to denser and smoother 3D printed structures. A certain degree of complexity is also achievable. Moreover, the 3D-LBL strategy is preferred over than 3D-CJD due to the higher degree of repeatability and control over printing.

With respect to the not diluted solution, Fig. 2**a** specifically shows a 3D-CJD dendritic-like pillar with significant overspray. Printing was barely repeatable. Fig. 2**b** instead depicts well defined and repeatable 3D-LBL structures, such as a tubular shape with a diameter of 2 mm, and frost/tree-like pillars with a diameter base of ~ 100 µm.

Alternatively, Fig. 2**c-d** report 3D microstructures achieved with a diluted ink (AgNPs:DI water ratio of 1:4). In such condition, cones or branches are obtained with the 3D-CJD technique (Fig. 2**c**). Particularly, the branch structure is built up from the cone structure by keeping the nozzle steady and continously jetting the aerosol on the substrate. Vertically aligned cones are approximately 374 µm height, with 3 < AR < 12 based on the applied focusing

ratio, R_f. For instance, cones with a base diameter of 141.47 ± 11. 81 μm and a tip diameter of 31.65 ± 2.59 μm are obtained at R_f = 4, with a medium process reproducibility. Instead, poly-branches are created from a mono-branch which subsequently divides in multi-branches (i.e. leaf-like structure) during CJD (printing time < 3 secs), but at a low reproducibility in the meaning that no control can be imposed on the direction of branch generation, resulting in similar, but not repeatable, structures. Among the three inks investigated, this particular building-up phenomenon has been achieved only with the AgNPs ink, most probably due to its low surface tension and viscosity, along with the nature of the spherical metal NPs. Instead, by 3D-LBL, array (such as 6x4) of vertically aligned micropillars can be easily disposed. The average height is 960.42 ± 37.69 μm (equal to 50 printed layers), the diameter 47.74 ± 5.62 μm, and the AR is ca. 20 (Fig. 2**d**). In this case, the pillars present a hollowed structure (inner diameter < 20 μm) and the printed pattern is clearly visible, with a growth rate of ∼ 19 μm/layer. A substantial OS is also visible at the bottom of the printed pillars. Accordingly, it is recommended to maintain a minimum interpillars distance of 200 μm to avoid interconnections. These 3D micropillars are obtained when the platen temperature is increased from $T_{CJD,\ AgNPs}$ = 40 °C to $T_{LBL,\ AgNPs}$ = 100 °C, initiating an in-loco pre-sintering process. Compared to 3D-CJD, a smaller nozzle $Ø_{LBL,\ AgNPs}$ = 100 μm, a higher $CGF_{\ LBL,\ AgNPs}$ = 18 sccm, a lower $R_{f,\ LBL,\ AgNPs}$ = 1.67 and a lower print speed, $s_{\ LBL,\ AgNPs}$ = 0.4 mm/*sec*, are selected to obtain the most controllable LBL jet deposition.

3.2. PEDOT:PSS-based ink

The second type of ink explored is PEDOT:PSS-based. Table 2 summarises the print parameters. As reported in Fig. 3, only the own-formula combined with the adoption of the 3D-LBL technique were successfully printed in 3D structures. Fig. 3**a-b** show the 3D-CJD of micropillars bended more than 130° printed with both inks and at a low process reproducibility. Instead, Fig. 3**c** reports an array of 3D-LBL printed micropillars, with an average.

height of 322.69 ± 7.86 μm (50 layers), a diameter of 45.52 ± 2. 22 μm, for a maximum AR = 7. These 3D PEDOT:PSS-based pillars present a growth rate of ∼ 6.5 μm/layer, and a compact internal structure. These structures were 3D printed at the same print speed of the AgNPs-based diluted ink, but the achievable accuracy was lower. The possibility to achieve poly-branches was also rare, most likely due to the higher ink viscosity. More complex 3D patterns, such as the KU Leuven logo, were printed at a font size of ∼ 70 μm (Fig. 3**d**). The platen temperature was set at $T_{PEDOT:PSS}$ = 80 °C, since lower ones have not allowed the building up of 3D structures, while higher ones have produced deformed shapes.

3.3. Collagen-based ink

The third type of ink assessed for their potential in 3D AJ® printing is collagen-based, and more specifically a Col-HAp ink with and without the addition of 1 M glycerol. Table 2 reports the print parameters used. The bed temperature was kept at $T_{\ Collagen}$ = 37 °C to mimic physiological conditions. As shown in Fig. 4, both inks are nicely printable in 3D structures, but the addition of 1 M glycerol to the solvent mixture results in more complex prints. Again, the 3D-LBL strategy gives better results and higher reproducibility than the 3D-CJD one. The collagen ink is 3D-CJD printed in the shape of dense and elongated micro-cones (AR ∼ 4) (Fig. 4**a**) and 3D-LBL printed as hollowed pillars with an AR = 2.6, height of 216.5 ± 8.2 μm, and width of 84.1 ± 4.6 μm (Fig. 4**b**). Besides, a PW approach was used to print a pyramid-like structure to resemble a lattice unit (Fig. 4**c**). Finally, Fig. 4**d** and Fig. 4**e** report an array of 3x3 pillars and the university logo, both printed using the 3D-LBL strategy.

4. Discussion and conclusions

This paper covers the fabrication of 3D microstructures by means of the AJ®P technology, with focus on the effects of inks composition and print strategies. Three functional inks among AgNPs-, PEDOT:PSS-, and collagen-based solutions, are here investigated according to different print strategies, that is 3D CJD, LBL, and PW printing of structures with at least an AR = 1 and in a fast printing time (≤30 mins). For all cases, the typical conditions for a satisfactory AJ®P deposition are defined as: i) stable aerosol generation, ii) optimal evaporation rate of the in-flight jet, and iii) adequate ink-substrate interaction. Thus, the selection of the (co–)solvents system plays a fundamental role, which must balance high and low volatile solvents in order not to exceed a certain concentration margin (different from case to case), beyond which the printed ink becomes too wet (2D printing).

Among the three inks, the 3D-LBL AgNPs-based ink demonstrated the best ability to print reproducible 3D microstructures (pillars) at the highest ARs and resolutions. This is caused by its high loading particle, which can be fine-tuned (through dilution) for 2D and 3D printing. In the case of 3D printing with the not diluted solution, the solid particle content (∼50 wt%) is too high compared to the co-solvent concentration (≤20 v/v%), leading to a faster evaporation rate in the transport and in-flight jet, eventually causing the deposition of rough, dendritic-like structures. Instead, the dilution allowed the printing of a wetter aerosol, reducing the ink drying effect. AgNPs-based 3D microstructures can be applied in the PE fabrication of highly conductive, cost-effective, and customizable 3D passive and active elements for

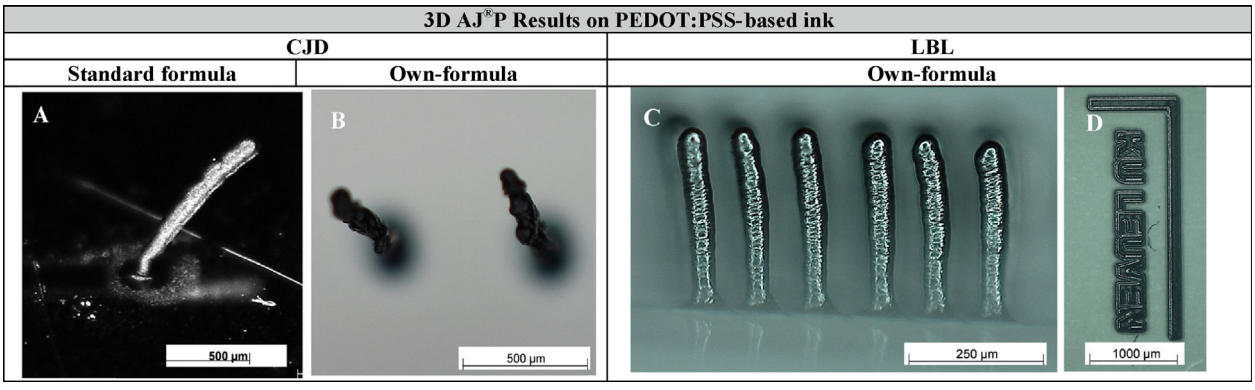

Fig. 3. Results for the 3D AJ®P of microstructures for PEDOT:PSS-based ink, along with print strategy and characterization.

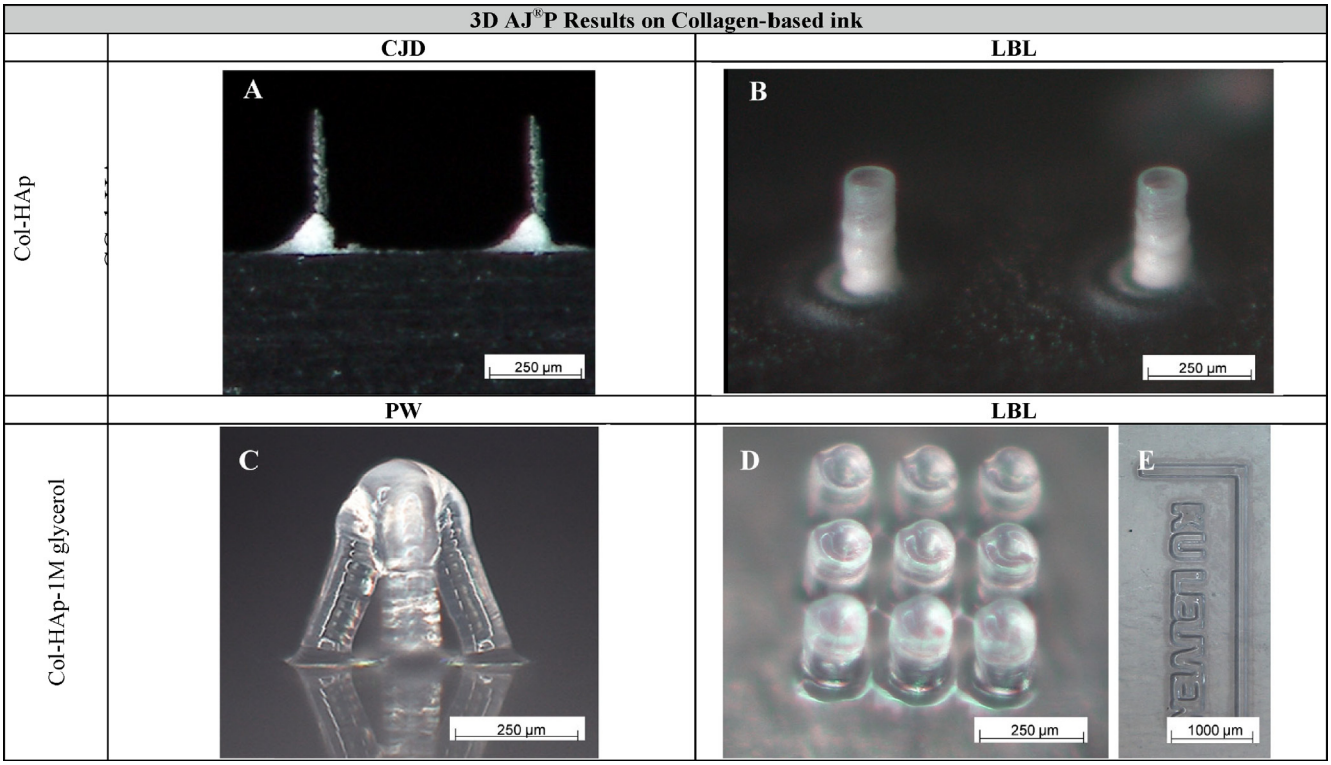

Fig. 4. Results for the 3D AJ®P of microstructures for Collagen-based ink, along with printing strategy and ink formulation.

energy harvesting devices, batteries, (optoelectronic) sensors, and so on. If properly encapsulated, these structures can be also exploited in life science applications, such as bioelectronic sensing, lab-on-a-chip, and tissue engineering devices. As demonstrated by the same authors, the release of Ag^+ ions in medium culture, from exposed AgNPs printed patterns, indeed generates high levels of cytotoxicity on different cellular lineages [20]. Therefore, in the context of life science, the use of biocompatible inks is preferable, such as PEDOT:PSS- and collagen-based inks. PEDOT:PSS showed good potential as bio-conductive 3D AJ®P ink for multi-functional applications in the field of bioelectronics. Particularly, the addition of polyethylene glycol (PEG) and carboxymethyl cellulose (CMC) to the standard PEDOT:PSS formulation, supported the build-up of well-defined 3D micropillars, due to their action as binders and loading contents. The ink has been also proven biocompatible by the same authors in preliminary direct rATP cytotoxicity assays on neural stem cells (NSCs), till 72 h [21].

Also collagen exhibits good biocompatibility, being the most abundant protein in mammals. Due to the presence of specific cellular recognition amino acid sequences, collagen indeed plays a crucial role in cellular processes, such as cell attachment and proliferation. For instance, collagen type I and II inks have recently been AJ® printed to produce dense collagen films for applications in corneal tissue engineering.[19] However, printing of 3D structures is new to this respect. In order to mimic the composition of human bone tissue, HAp nano-particles (<200 nm) were incorporated into the ink in a biomimetic ratio (1:2 Col:HAp ratio). As already mentioned before, the solid loading of the inks plays a crucial role in 3D printing using AJ®P. Hence, it was hypothesized that the addition of HAp nano-particles could improve the 3D printing behaviour of the collagen composite inks. The collagen-HAp ink allowed for the printing of hollowed pillars, nevertheless, more complex structures could not be fabricated using this ink composition. Hence, the effect of adding glycerol was assessed, as it was believed that adding a solvent with low volatility could aid in the build-up of 3D structures. Indeed, the addition of 1 M of glycerol allowed for the fabrication of more complex structures, such as the pyramid shown in Fig. 4**c**. These pyramids could be used as unit-cells for more complex lattice structures. It should be noted, however, that the addition of glycerol resulted in thicker walls for the hollow pillars, closing the central channel. Hence, adding glycerol improved the 3D printing capabilities, but reduced the printing resolution and accuracy. It is suggested that adding a solvent with low volatility, such as glycerol, aids in the build-up of material by keeping the ink hydrated. Moreover, as glycerol has a higher viscosity compared to the aqueous collagen solution, it ensures cohesion of the structure upon deposition, as the viscosity of the deposited droplets increases while drying out in the in-flight jet, resulting in a gel-like liquid being deposited. This combined effect of wetting the ink and increasing the viscosity while drying, eventually lead to the printing of 3D structures.

To summarize, the AJ®P technique can be considered an enabling technology to realize high AR 3D bio(electrical) microstructures. An ideal 3D U-AJ®P ink should have: i) standard U-AJ®P ink requirements, ii) a solid (metal, polymeric, ceramic) loading content in the range of 10–25 wt% and additional binders, iii) a co-solvent system which comprises humectants for a balanced evaporation rate, iv) controlled print parameters, such as T, R_f, and s. Indeed, all inks require a low s and a R_f in the range of [1.66–4], and particle loaded inks at $T \geq 40$ °C. Besides, a 3D-LBL strategy is preferred for vertically-aligned, multi-layered arrays ($AR_{AgNPs} \sim 20$, $AR_{PEDOT:PSS} \sim 7$, $AR_{Collagen} \sim 3$), while 3D- PW/CJD for complex geometries.

Due to a currently limited amount of AJ®P inks in the market (only addressed to PE), this study gives the basis to develop custom-made 3D AJ®P inks, also prompt to be sustainable, biodegradable, and recyclable. Based on the ink chosen, 3D microstructures can be potentially exploited for a vast range of low-cost prototypes in life science (tissue engineering, bioelectronic interfaces), electronics, and MEMS. Future studies will be

focused on a quantitave characterization of the process and materials, such as the significance of boiling temperature and vapour pressure over the resulting structure. Moreover, for the collagen inks, a crosslinking approach will be studied, being necessary to improve the mechanical properties of the printed structures. Furthermore, the use of methacrylated collagen (ColMA) combined with UV-irradiation will be assessed for 3D AJ®P.

Data availability

Data will be made available on request.

Declaration of Competing Interest

The authors declare that they have no known competing financial interests or personal relationships that could have appeared to influence the work reported in this paper.

Acknowledgements

The authors gratefully acknowledge the Research Foundation Flanders (FWO, Belgium) for the doctoral fellowship granted to Miriam Seiti, 1SB1120N, and Olivier Degryse, 1S86620N.

References

[1] J. Xu, X. Wang, C. Wang, L. Yuan, W. Chen, J. Bao, Q. Su, Z. Xu, C. Wang, Z. Wang, D. Shan, B. Guo, A review on micro/nanoforming to fabricate 3D metallic structures, Adv. Mater. 33 (6) (2021) 2000893, https://doi.org/10.1002/adma.202000893.

[2] M. Vaezi, H. Seitz, A review on 3D micro-additive manufacturing technologies, Springer, 2013.

[3] J. Yunas, B. Mulyanti, I. Hamidah, M. Mohd Said, R.E. Pawinanto, W.A.F. Wan Ali, A. Subandi, A.A. Hamzah, R. Latif, B. Yeop Majlis, Polymer-based MEMS electromagnetic actuator for biomedical application: a review, Polym. 12 (5) (2020) 1184, https://doi.org/10.1002/adma.202000893.

[4] Y. Qian, D.J. Magginetti, S. Jeon, Y. Yoon, T.L. Olsen, M. Wang, J.M. Gerton, H.P. Yoon, Heterogeneous optoelectronic characteristics of Si micropillar arrays fabricated by metal-assisted chemical etching, Sci. Reports 10 (1) (2020), https://doi.org/10.1038/s41598-020-73445-x.

[5] Y.G. Park, H. Min, H. Kim, A. Zhexembekova, C.Y. Lee, P.JU. Three-Dimensional, High-resolution printing of carbon nanotube/liquid metal composites with mechanical and electrical reinforcement, Nano Lett. 19 (8) (2019) 4866–4872, https://doi.org/10.1021/acs.nanolett.9b00150.

[6] F. Jannah, J.H. Kim, J.W. Lee, J.M. Kim, J.M. Kim, H. Lee, Immobilized polydiacetylene lipid vesicles on polydimethylsiloxane micropillars as a surfactin-based label-free bacterial sensor platform, Front. Mater. 5 (2018) 57, https://doi.org/10.3389/fmats.2018.00057.

[7] J. Wang, H. Xiong, T. Zhu, Y. Liu, H. Pan, C. Fan, X. Zhao, W.W. Lu, Bioinspired multichannel nerve guidance conduit based on shape memory nanofibers for potential application in peripheral nerve repair, ACS Nano 14 (10) (2020) 12579–12595.

[8] A. Yadav, N. Verma, Efficient hydrogen production using Ni-graphene oxide-dispersed laser-engraved 3D carbon micropillars as electrodes for microbial electrolytic cell, Renew. Energy 138 (2019) 628–638, https://doi.org/10.1016/j.renene.2019.01.100.

[9] J. Machiels, A. Verma, R. Appeltans, M. Buntinx, E. Ferraris, W. Deferme, Printed electronics (PE) as an enabling technology to realize flexible mass customized smart applications, Procedia CIRP 96 (2021) 115–120, https://doi.org/10.1016/j.procir.2021.01.062.

[10] M. Seiti, P.S. Ginestra, R.M. Ferraro, S. Giliani, R.M. Vetrano, E. Ceretti, E. Ferraris, Aerosol Jet® printing of Poly(3,4-Ethylenedioxythiophene): Poly (Styrenesulfonate) onto micropatterned substrates for neural cells in vitro stimulation, Int. J. Bioprinting 8 (1) (2022) 504.

[11] N.X. Williams, N. Watson, D.Y. Joh, A. Chilkoti, A.D. Franklin, Aerosol jet printing of biological inks by ultrasonic delivery, Biofabrication 12 (2) (2020), https://doi.org/10.1088/1758-5090/ab5cf5 025004.

[12] M.S. Saleh, C. Hu, R. Panat, Three-dimensional microarchitected materials and devices using nanoparticle assembly by pointwise spatial printing, Sci. Adv. 3 (3) (2017) e1601986, https://doi.org/10.1126/sciadv.1601986.

[13] S. Zips, L. Grob, P. Rinklin, K. Terkan, N.Y. Adly, L.J.K. Weiß, D. Mayer, B. Wolfrum, Fully printed μ-needle electrode array from conductive polymer ink for bioelectronic applications, ACS Appl. Mater. Interfaces 11 (36) (2019) 32778–32786, https://doi.org/10.1021/acsami.9b11774.

[14] A. Hohnholz, K. Obata, Y. Nakajima, J. Koch, M. Terakawa, O. Suttmann, et al., Hybrid UV laser direct writing of UV-curable PDMS thin film using aerosol jet printing, Appl. Phys. A Mater. Sci. Process. 125 (2) (2019) 1–6, https://doi.org/10.1007/s00339-018-1902-0.

[15] N.G. Di Novo, E. Cantù, S. Tonello, E. Sardini, M. Serpelloni, Support-material-free microfluidics on an electrochemical sensors platform by aerosol jet printing, Sensors 19 (8) (2019), https://doi.org/10.3390/s19081842.

[16] E.B. Secor, Principles of aerosol jet printing, Flex Print Electron 3 (3) (2018) 035002, https://doi.org/10.1088/2058-8585/aace28.

[17] N.J. Wilkinson, M.A.A. Smith, R.W. Kay, R.A. Harris, A review of aerosol jet printing—a non-traditional hybrid process for micro-manufacturing, Int. J. Adv. Manuf. Technol. 105 (11) (2019) 4599–4619, https://doi.org/10.1007/s00170-019-03438-2.

[18] B.A. Williams, N.D. Trejo, A. Wu, C.S. Holgate, L.F. Francis, E.S. Aydil, Copper–zinc–tin–sulfide thin films via annealing of ultrasonic spray deposited nanocrystal coatings, ACS Appl. Mater. Interfaces 9 (22) (2017) 18865–18871, https://doi.org/10.1021/acsami.7b04414.

[19] R. Gibney, E. Ferraris, Bioprinting of collagen type I and II via aerosol jet printing for the replication of dense collagenous tissues, Front. Bioeng. Biotechnol. 9 (2021) 1–12, https://doi.org/10.3389/fbioe.2021.786945.

[20] M. Seiti, P. Ginestra, R.M. Ferraro, E. Ceretti, E. Ferraris, Nebulized jet-based printing of bio-electrical scaffolds for neural tissue engineering: a feasibility study, Biofabrication 12 (2) (2020), https://doi.org/10.1088/1758-5090/ab71e0 025024.

[21] Seiti M, Ferraro RM, Ginestra P, Ceretti E, Ferraris E. Development of a bioelectrical ink for Aerosol Jet® Printing of 3D microstructures. *Wollongong, Australia* (online): 2021.